Journal of Power Sources 240 (2013) 314–322

Contents lists available at SciVerse ScienceDirect

Journal of Power Sources

journal homepage: www.elsevier.com/locate/jpowsour

Development of a piezoelectric proton exchange membrane fuel cell stack (PZT-Stack)

H.K. Ma*, H.M. Cheng, W.Y. Cheng, F.M. Fang, W.F. Luo

Department of Mechanical Engineering, National Taiwan University, Taipei, Taiwan

HIGHLIGHTS

- An innovative pseudo-bipolar design for a PZT-Stack with three bi-cells has been successfully developed.
- The maximum power density is 0.1874 W cm^{-2} and 0.1765 W cm^{-2} in the electrical parallel and cascade configuration, respectively.
- The PZT-Stack does not exhibit open circuit behavior even if one of the component cells fails in the electrical cascade configuration.

ARTICLE INFO

Article history:
Received 23 October 2012
Received in revised form
25 February 2013
Accepted 27 March 2013
Available online 16 April 2013

Keywords:
Bi-cell
Piezoelectric device
Proton exchange membrane fuel cells
Stack
Power

ABSTRACT

Previous studies report that bi-cell piezoelectric proton exchange membrane fuel cells with a nozzle and a diffuser have been successfully developed, and this pseudo-bipolar design is expected to benefit the future development of the piezoelectric stack (PZT-Stack). In this study, an innovative PZT-Stack design composed of three L-PZT-D-type bi-cells contains a total reaction area of 24 cm^2 with a diffuser angle (θ) of 10°, a channel path (L) of 5.63 mm, and a channel opening width (D) of 1 mm. To optimize the performance of the PZT-Stack, the module is investigated under various operating conditions, including the PZT vibration frequency, the cell temperature, the relative humidity in the anode, the type of electrical circuit, and the type of intake module on the anode. The stability and the performance of a PZT-Stack with a degraded membrane electrode assemblies (MEA) are analyzed. Although the degraded working mode lowers the performance of the PZT-Stack, the module is still able to function consistently and deliver positive power. The maximum net power of the PZT-Stack was 3.8627 W under a PZT frequency of 60 Hz, and a cell temperature of 50 °C in a parallel electrical circuit.

1. Introduction

Because air-pumping proton exchange membrane fuel cells (AP-PEMFCs) require fewer auxiliary components (e.g., compressors, humidifiers, and heat exchangers) to support their performance, these devices have attracted attention due to their small structure and minimum balance of plant (BOP). For portable AP-PEMFC applications, the air supply device should be small in size, provide sufficient airflow, and require low power consumption. Among the various actuating methods, the piezoelectric actuator demonstrates good reliability, energy efficiency, and moderate volume displacement [1]. To improve the pumping flow rate, Olsson et al. [2], Ullmann [3], and Yang et al. [4] have investigated a piezoelectric valveless micropump system in which two chambers are placed in a series or parallel arrangement. The results show that the flow rate in a piezoelectric actuator can be controlled by altering the phase difference.

During operation of an AB-PEMFC, the membrane hydration plays an important role in proton conductivity. Furthermore, this hydration is affected by the conditions of the inlet gases and by the cell temperature [5,6]. Yi and Nguyen [7] showed that PEMFC performance was improved by anode humidification and by a positive differential pressure between the cathode and anode, factors that were also proven by the Nernst equation. Ge and Wang [8] indicated that a lower cell temperature, and hence a higher water condensation rate in the anode channels, can contribute to anode flooding.

The common methods of stacking consist of three types: bipolar, pseudo-bipolar, and mono-polar, for the pseudo-bipolar cell stack design it is easy to achieve high power by simple addition of more bi-cell units, but each bi-cell has to be filled with fuel and air separately. In the monopolar cell stack design a common gas flow

* Corresponding author. Tel.: +886 2 23629976; fax: +886 2 23632644.
E-mail address: skma@ntu.edu.tw (H.K. Ma).

0378-7753/$ – see front matter © 2013 Elsevier B.V. All rights reserved.
http://dx.doi.org/10.1016/j.jpowsour.2013.03.161

field is shared by a whole strip, when a single cell fails the stack performance will not be affected seriously. Monopolar cell stack design is suitable for applications in low power and high voltage devices because of its high internal resistance [9]. In this study, three pseudo-bipolar bi-cells are connected with external wires to achieve an electrical cascade or an electrical parallel configuration. Previous studies [10] have noted that flow in series from stack to stack can achieve higher total reactant utilizations.

Candusso et al. [11] indicated that there are four examples of topologies for a four-stack association that could be used as a power source for further applications. The FC modules can be autonomously or serially coupled to the load with the power converter or they can also be twin-coupled (a power module with two stacks in electrical cascade arrangement) to increase the voltage per module. Additionally, four FC stacks can be coupled together before connection to the power converter; this arrangement allows an increase in the total output voltage but exhibits a severe weakness when one or more FCs fails. In this study, because of the pseudo-bipolar design, the PZT-Stack does not become an open circuit even if one of the component cells fails in the electrical cascade. In addition, Bernardinis et al. [12] indicated that a diode can preclude a reverse current from flowing back to the stacks, and MOSFETs switches allow the coupling of an additional FC stack to maintain and control the total output voltage.

Previous studies [13–16] of a piezoelectric proton exchange membrane fuel cell with a nozzle and a diffuser (PZT-PEMFC-ND) have shown that a PZT device was able to solve these water-flooding problems in cathode and improve the cell performance. Therefore, the piezoelectric device in this work consists of an actuator type that pumps air into the cathode chamber, resulting in better performance and a higher current generation.

The study [17] also showed that improved PZT-PEMFC-ND cell performance could be obtained using an aspect ratio (AR) of 5.63 and a θ of 10°. Furthermore, a bi-cell piezoelectric proton exchange membrane fuel cell with a nozzle and a diffuser (PZT-PEMFC-ND bi-cell) has been developed, and its performance has been shown to be 1.6 times better than that of a single cell [18,19].

The objective of this study is to investigate a piezoelectric stack with three L-PZT-D type bi-cells shown in Figs. 1 and 2 under various operating conditions, including different PZT vibration frequencies, operating temperatures, electrical circuit arrangements (parallel or cascade), and intake modules on the anode. Moreover, to optimize the integrated system output, the performance of the three component bi-cells and the power consumption of the PZT device are taken into consideration.

2. A pseudo-bipolar design in the air-pumping PZT-Stack

2.1. Design of the PZT-Stack

In this study, the innovative design of the PZT-Stack consists of three L-PZT-D-type PZT-PEMFC-ND bi-cells; the pseudo-bipolar design was chosen for the PZT-Stack to deliver additional power. The pseudo-bipolar design of the bi-cell is composed of two outside anodes and two inside cathodes that share a common PZT vibrating device used to pump the airflow. This arrangement allows one PZT device to supply air to the two component cells and pump the produced water out of the cells, thus reducing the total power consumption, as shown in Fig. 1.

2.2. Actuation mechanism

In a PZT-Stack bi-cell, two diffuser elements are applied to induce a larger airflow rate, as shown in Fig. 2. The geometrical parameters of the diffuser affect the pump performance, including the diffuser angle (θ) and the aspect ratio (AR). Previous study [16] showed that the pump performance of PZT-PEMFC-ND is a function of geometry parameters, aspect ratio (AR) and diffuser angle (θ). In order to have optimal pump efficiency, a larger value for the diffuser angle (θ) should be chosen when the Reynolds number is decreasing. Previous study [18] also showed that the geometries of the nozzle/diffuser in the PZT-PEMFC-ND influence the I–V curve significantly and the performance improves when a smaller AR of 5.63 and a larger θ of 10° are used. In this study, the diffuser angle

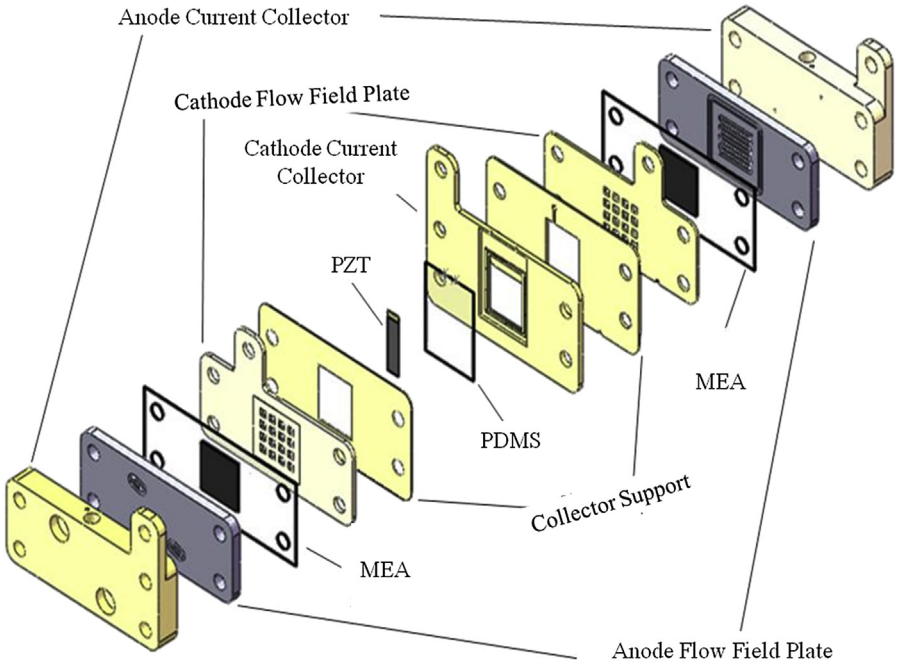

Fig. 1. An exploded drawing of the L-PZT-D-type bi-cell of the PZT-Stack.

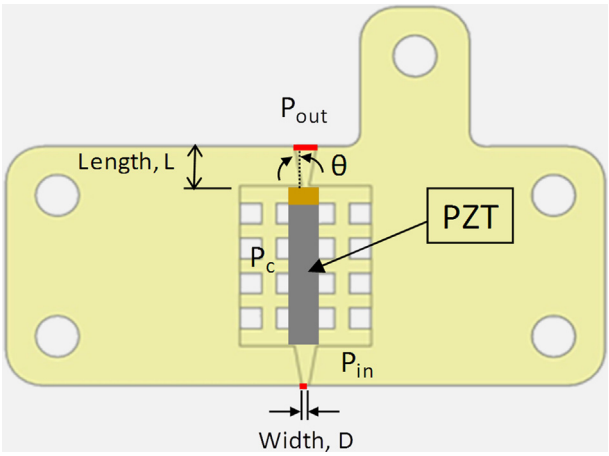

Fig. 2. The design of L-PZT-D-type bi-cell in cathode channel.

(θ) is 10°, the cathode channel path (L) is 5.63 mm and the channel opening (D) is 1 mm.

As shown in Fig. 3, the time variation method was applied for the following: pump mode ($P_c > P_{out} > P_{in}$), supply mode ($P_{out} > P_{in} > P_c$), and transition mode ($P_{out} > P_c > P_{in}$). In supply mode, the diaphragm moved outward and the cathode chamber volume increased, which caused the chamber pressure (P_c) to become lower than the atmospheric pressure (P_{in} and P_{out}) and, thus, the air was sucked into the chamber. In pump mode, the diaphragm moved inward and the cathode chamber volume decreased. Because the pressure inside the cell (P_c) was higher than the atmospheric pressure, the air was pushed into the catalyst layer and the water produced was pumped out of the cell. A transition mode occurred between the pump mode and the supply mode, when the outlet pressure was higher than the chamber and inlet pressures, $P_{out} > P_c > P_{in}$. The assumption was made that the inlet pressure, P_{in} is always smaller than the outlet pressure, P_{out} due to the nozzle/diffuser design.

To analyze the airflow rate of the PZT-Stack system, the control volume of the system was located inside the cathode chamber. The equation of motion for the PZT device was modeled as a sine function given by Eq. (1).

$$\vec{V}_{PZT} = \frac{d}{dt}[-\Lambda \times (\sin(2\pi f t))] \quad (1)$$

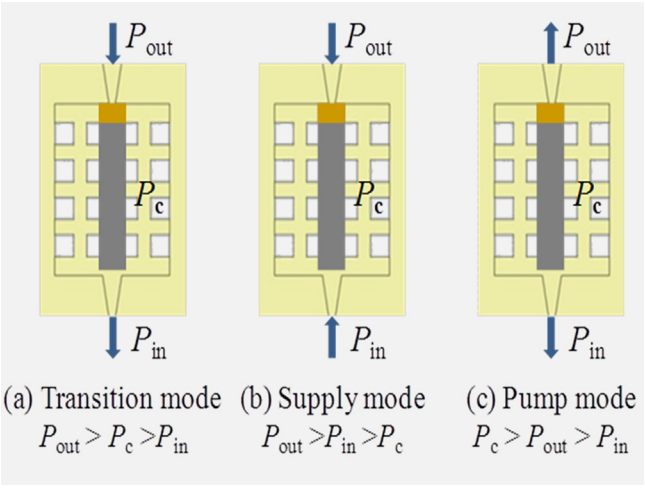

Fig. 3. The three flow modes during the PZT-actuating process.

Thus, using the Reynolds Transport Theorem and the continuity equation, the airflow rate can be written as Eq. (2):

$$Q = {}^{1}\Big/_{R}\frac{\partial}{\partial t}\int_{C\forall} P\Big/_{T} d\forall + \rho \vec{V}_{PZT} A_{PZT} \quad (2)$$

The inlet flow from the nozzle and the diffuser can be found using the diffuser element theory as follows Eqs. (3) and (4):

For the air inflow from top to bottom:

$$Q_{in,t} = C_n \sqrt{P_{out} - P_c} \quad (3)$$

For the air inflow from bottom to top:

$$Q_{in,b} = C_n \sqrt{P_c - P_{out}} \quad (4)$$

3. Experimental setup

Fig. 4 shows the test platform used to analyze the performance of the PZT-Stack. The PZT-Stack with three L-PZT-D-type bi-cells has a total reaction area of 24 cm^2 with a diffuser angle (θ) of 10°, a channel path (L) of 5.63 mm, and a channel opening width (D) of 1 mm. The hydrogen in the anode side is supplied by hydrogen storage, and six flow meters monitor the hydrogen flow rate in the different component cells. High-pressure hydrogen enters the humidifier before passing through the mass flow controller. The humidifier consists of a water tank with a heater that allows the reactant gas to pass at a specific temperature. Next, the hydrogen with water vapor is delivered to the PZT-Stack for an electrochemical reaction. Fig. 5(a) shows the parallel hydrogen intake module on the anode in the PZT-Stack. In parallel flow, the six component cells are supplied with a hydrogen flow rate 30 ml min^{-1}. Fig. 5(b) shows a series hydrogen intake module on the anode in the PZT-Stack. In series flow, Cell 1 is initially supplied with 180 ml min^{-1} of hydrogen flow; next, the reacted gas and un-reacted hydrogen flow into the next component cell, etc.

The PZT device controls the airflow on the cathode side. A functional generator is used to deliver sine wave signals to activate the PZT vibration. The signals from the function generator are sent to an amplifier for magnification and are subsequently transmitted through the signal wires to the middle of the module. A power meter is connected to the output terminal of the amplifier to measure the power consumption of the PZT device.

In this study, the constant voltage mode is chosen when the bi-cell is arranged in an electrical parallel configuration. The pseudo-bipolar design is used as the common cathode collector, and the collector support is constructed from gold-plated copper plate to allow conduction between the two component cells. Furthermore, the three bi-cells shown in Fig. 4 are arranged in an electrical parallel or electrical cascade configuration by connections of external wires. Fig. 6(a) shows the schematic of the electrical parallel configuration of the PZT-Stack. In this configuration, the anodes of the three bi-cells are connected by external wires to the negative pole of the electronic load, and the cathodes of the bi-cells are connected to the positive pole of the electronic load to form the electrical parallel configuration. Fig. 6(b) shows the schematic of the electrical cascade of the PZT-Stack. The constant current mode of the electronic load is chosen when the bi-cell is arranged in the electrical cascade configuration. The common cathode collector of Bi-cell #1 is connected to the anode of Bi-cell #2. Similarly, the common cathode collector of Bi-cell #2 is connected to the anode of Bi-cell #3 etc. to form the electrical cascade.

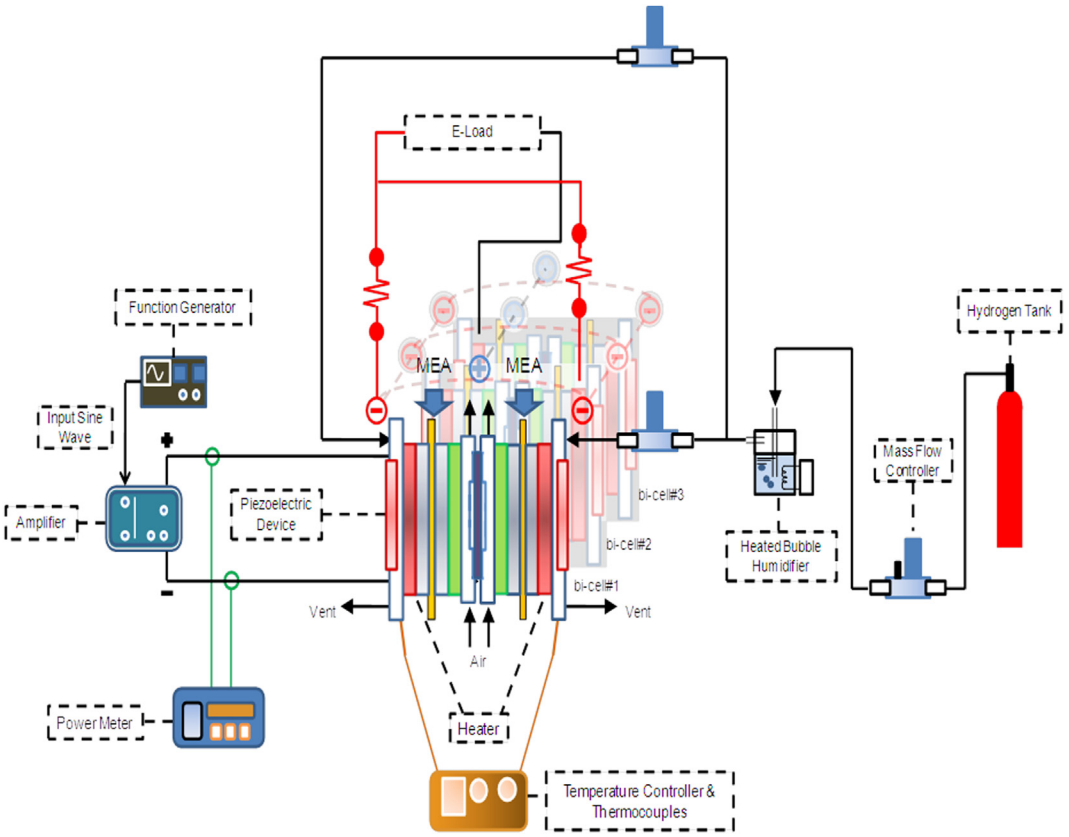

Fig. 4. Schematic of the test platform for operating the PZT-Stack.

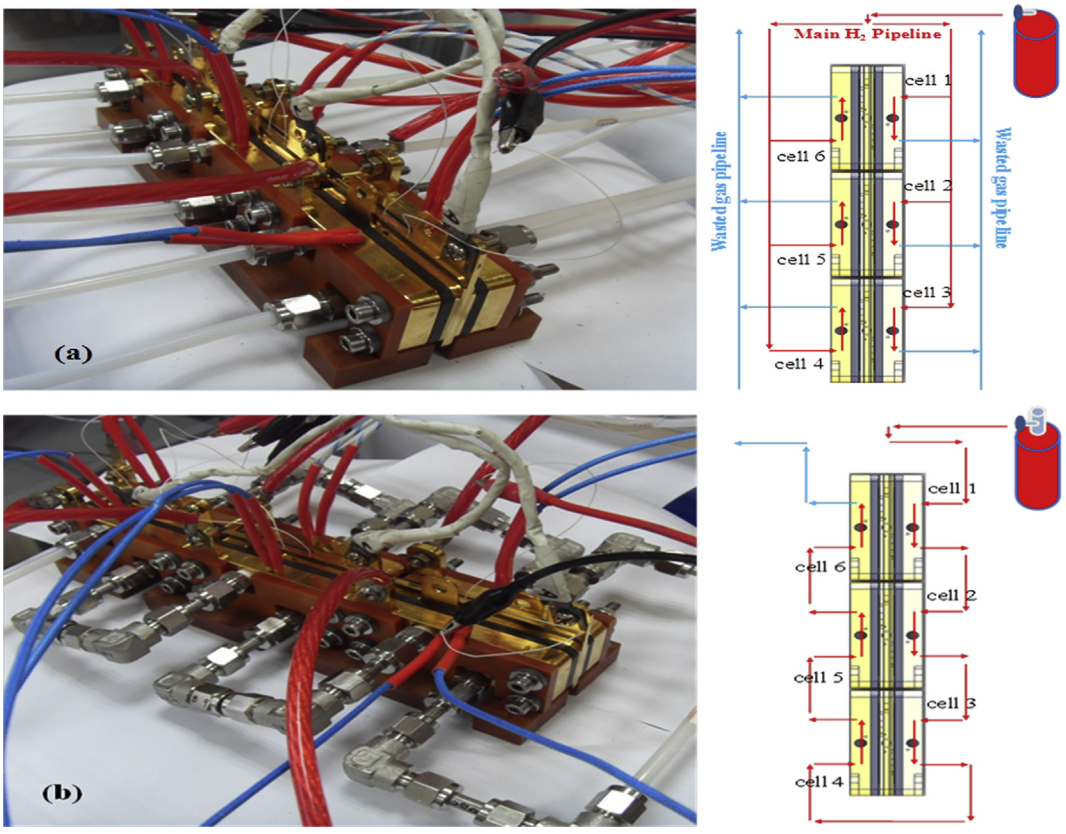

Fig. 5. Schematic of (a) parallel fuel intake module and (b) series fuel intake module on anode of the PZT-Stack.

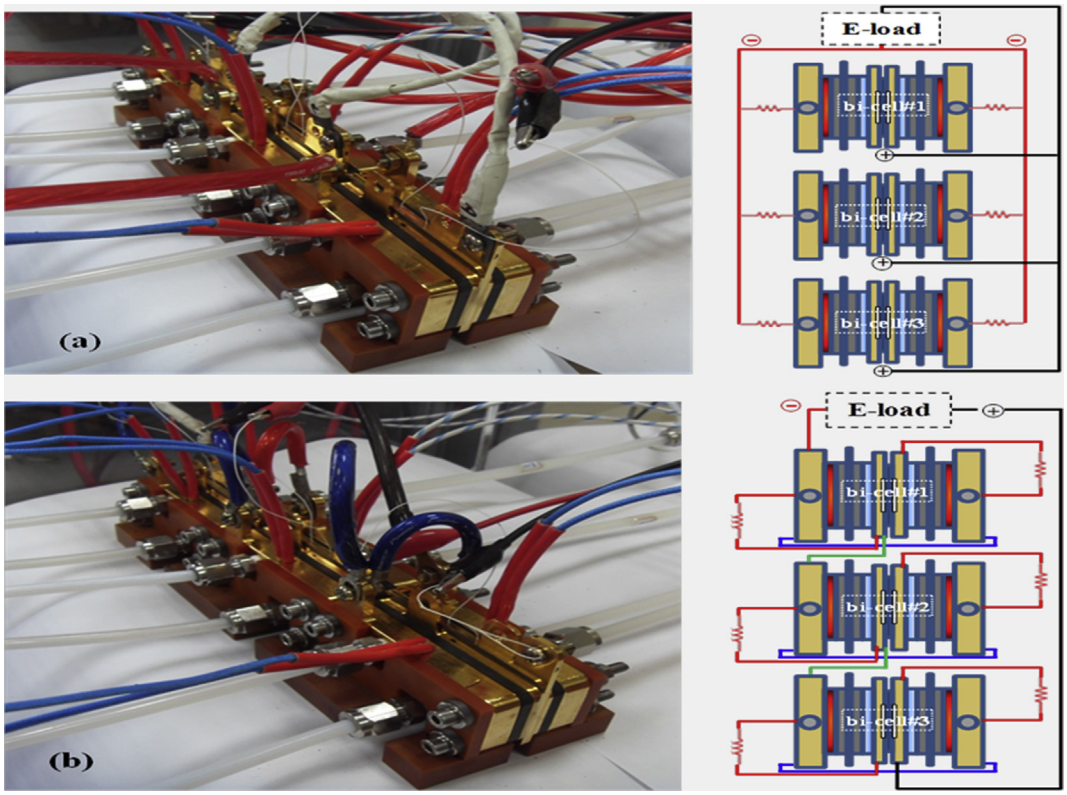

Fig. 6. Schematic of (a) electrical parallel configuration and (b) electrical cascade configuration in the PZT-Stack.

A DC electronic load was used to simulate the electronic loading of voltage and current. In the electrical cascade configuration, a constant current mode was chosen, and the polarization curve was obtained by increasing the current from 0 A to 4 A by 0.4 A every 10 min. In the electrical parallel arrangement, a constant voltage mode was chosen, and the polarization curve was obtained by decreasing the open-circuit voltage to 0.1 V from 0.2 V every 10 min, with control via LabVIEW software. Furthermore, current shunts with data acquisition modules measured the voltage of the six component cells in the electrical cascade to obtain the current density of the six component cells in the electrical parallel configuration.

4. Results and discussion

In this study, the influence of the PZT vibration frequency, cell temperature and anode relative humidity were investigated to determine the performance of the L-PZT-D-type bi-cell with a diffuser angle of 10° and an aspect ratio of 5.63. The optimal performance of the entire PZT-Stack was analyzed under conditions with the hydrogen intake modules on the anode and the circuit modules in electrical parallel and electrical cascade configuration. To estimate the net power of the PZT-Stack, the stack performance was considered with respect to the power consumption of the PZT devices. Moreover, the stability and performance of a PZT-Stack with a degraded MEA were also discussed.

4.1. Influence of PZT vibration frequencies

The PZT vibration frequency is an important parameter for actuation of the airflow in the cathode chamber. When the PZT device attached to a PDMS film is operated at its harmonic frequency, the bi-cell performance can be improved by intake of additional air into the chamber and ejection of additional produced water out of the chamber. Fig. 7 shows the performance of an L-PZT-D-type bi-cell operated under various PZT vibration frequencies. The result shows that the performance of the bi-cell increases as the frequencies increases from $f = 0$ Hz to $f = 90$ Hz because additional air is sucked into the chamber and additional produced water is pumped out of the cathode side. However, the performance of the bi-cell decreases between $f = 90$ Hz and $f = 150$ Hz because these frequencies lie outside of the harmonic frequency range of the PZT device. When the frequencies lie outside of the harmonic frequency range, the vibrating amplitude of PZT is decreasing to supply less airflow and drops the cell

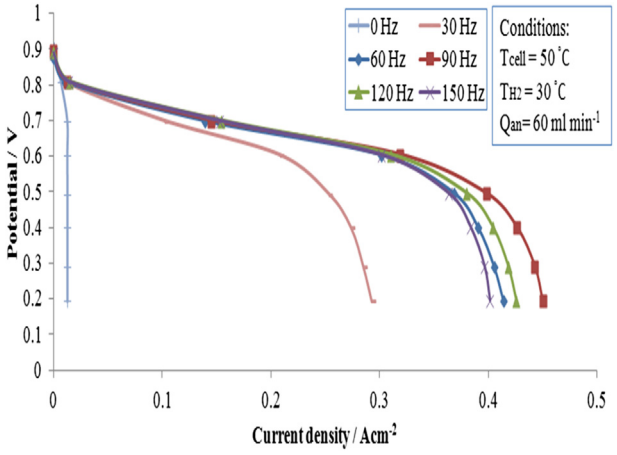

Fig. 7. The performance of an L-PZT-D-type bi-cell operated under various PZT vibration frequencies.

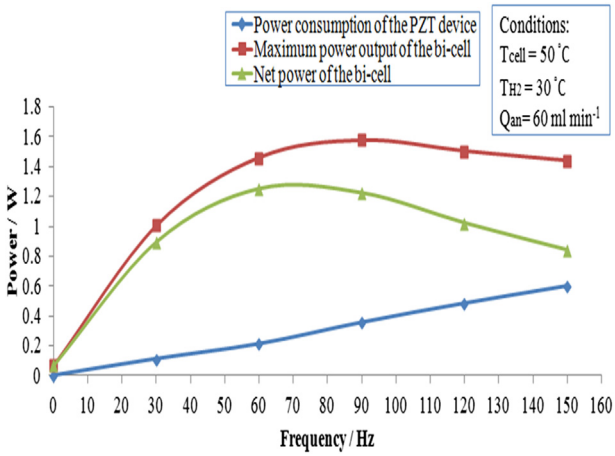

Fig. 8. The net power of the bi-cell under different PZT vibration frequencies.

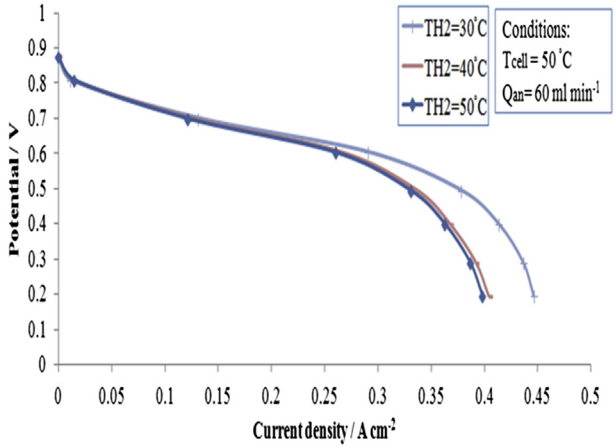

Fig. 10. The performance of L-PZT-D-type bi-cell with different hydrogen humidification temperatures (T_{H_2}).

performance. Although the performance of the bi-cell at $f = 90$ Hz is better than that at $f = 60$ Hz, the net power is higher at $f = 60$ Hz if the power consumption of the PZT device is considered, as shown in Fig. 8.

4.2. Influence of the cell temperature and the anode relative humidity

Previous studies have indicated that an appropriate increase in cell temperature is an effective parameter for ensuring high performance. Fig. 9 shows the performance of the L-PZT-D-type bi-cell under different operating temperatures ranging from 30 °C to 60 °C with a hydrogen relative humidity of 100%, $Q_{An} = 60$ ml min^{-1}, and $f = 60$ Hz. As the temperature increases from 30 °C to 50 °C, the cell performance also increases because a high temperature improves the chemical reaction rate. Furthermore, additional water is generated to hydrate the membrane, thereby decreasing the ohmic loss. However, the bi-cell performance does not increase significantly with continued increases in temperature. The current density and cell performance both decrease as the temperature increases from 50 °C to 60 °C because lower anode relative humidity induces a larger back diffusion of water which is unfavorable for the electron transfer. In addition, the current density and the cell performance decrease as the cell temperature increases from 50 °C to 60 °C because a larger activation loss is induced.

Fig. 10 shows the performance of the L-PZT-D-type bi-cell under different hydrogen humidification temperatures ranging from 30 °C to 50 °C. To analyze the influence of different relative humidity values in the anode, the bi-cell temperature was fixed at 50 °C; the performance at $T_{H_2} = 30$ °C was shown to be superior because a lower anode relative humidity contains less water vapor and therefore incurs less concentration losses. Therefore, the optimal performance will be obtained at $T_{H_2} = 30$ °C and $T_{cell} = 50$ °C.

4.3. Influence of the PZT-Stack circuit module

Fig. 11 shows the I–V curves of the bi-cells and the PZT-Stack in the electrical parallel configuration with parallel flow, $T_{H_2} = 30$ °C, $T_{cell} = 50$ °C, and $f = 60$ Hz. Bi-cells #1 through #3 produce a current density of 0.4975 A cm^{-2}, 0.411 A cm^{-2}, and 0.4675 A cm^{-2}, respectively, at constant load voltage of 0.2 V.

Fig. 12 shows the I–V curves of the bi-cells and the PZT-Stack in the electrical cascade configuration with parallel flow. In the electrical cascade, if the load current is set beyond the current limitation of any bi-cell, the cell voltage will drop to zero. According to the result in Fig. 12, Bi-cell #2 begins to generate a lower current density than that of the other cells when the load voltage approaches 0.5 V. Finally, the load current of 3.6 A exceeds the current limitation of Bi-cell #2, and therefore its voltage drops to zero.

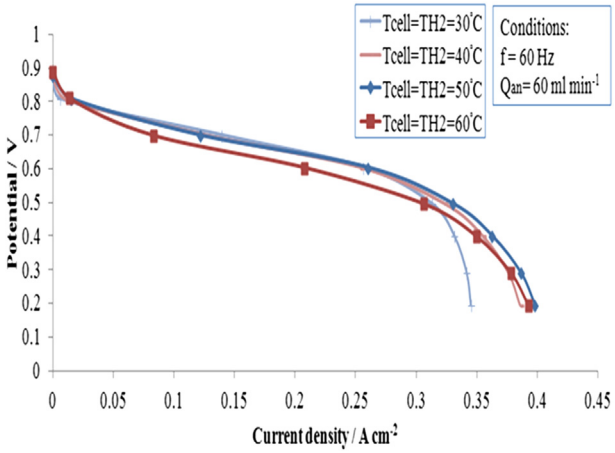

Fig. 9. The performance of L-PZT-D-type bi-cell at various cell temperatures (T_{cell}).

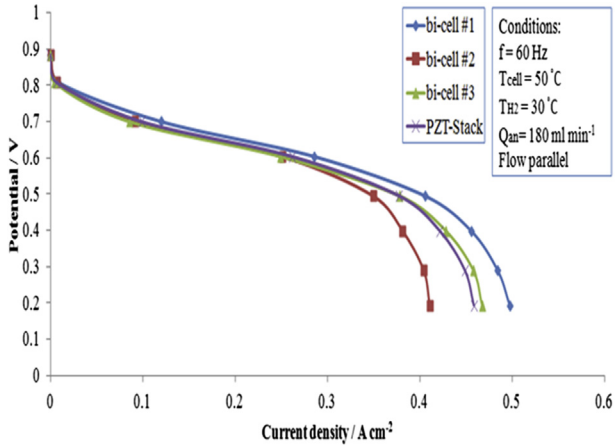

Fig. 11. The performance of PZT-Stack in electrical parallel configuration.

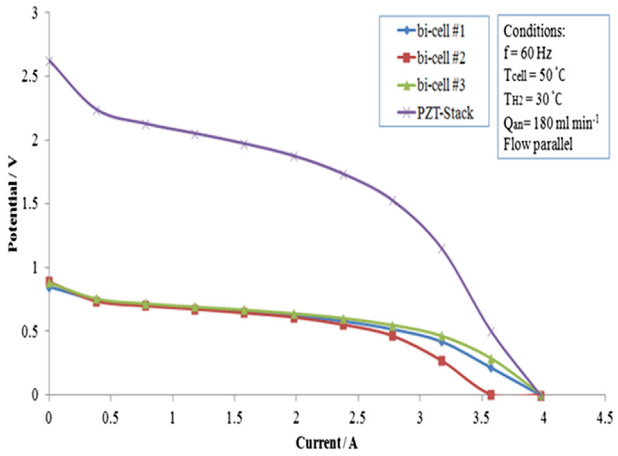

Fig. 12. The performance of PZT-Stack in electrical cascade configuration.

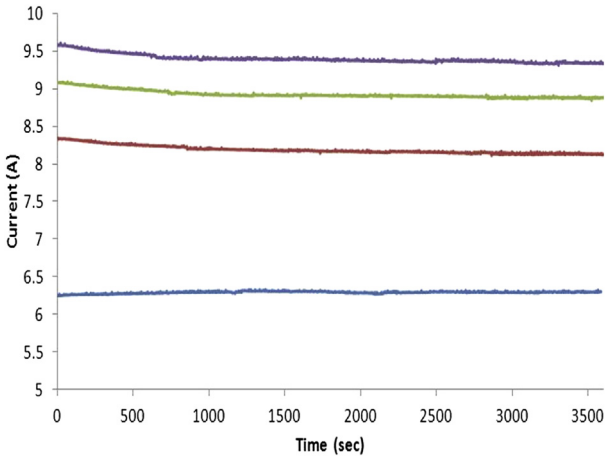

Fig. 14. The current stability of the PZT-Stack under various constant load voltages, T_{H_2} = 30 °C, T_{cell} = 50 °C, and f = 60 Hz with electrical parallel configuration.

Under different circuit modules of the PZT-Stack, the maximum power density is 0.1874 W cm^{-2} in the electrical parallel configuration and 0.1765 W cm^{-2} in the electrical cascade configuration.

4.4. Influence of intake module on anode

Fig. 13 shows the I–V curves of the PZT-Stack for different intake modules in the electrical parallel configuration. The performances of the PZT-Stack under series and parallel flow display slight differences in the regions of ohmic loss and concentration loss. The results show that the performance of the PZT-Stack under series flow is slightly poorer than that under parallel flow. In series flow, the fuel received by Cells 2 through 6 is composed of unreacted hydrogen and reacted gas instead of pure hydrogen, and this may cause additional concentration losses in the anode channel. For the different intake modules, the maximum power densities of the PZT-Stack under series and parallel flow are 0.1874 W cm^{-2} and 0.1652 W cm^{-2}, respectively.

4.5. Stability of the PZT-Stack

Fig. 14 shows the I–t curves of the PZT-Stack at different constant load voltages in the electrical parallel configuration, with T_{H_2} = 30 °C, T_{cell} = 50 °C, and f = 60 Hz. The stability of the output current over 1 h is analyzed, and observations show that certain performance differences exist under various load voltages of the PZT-Stack. At a constant load voltage of 0.6 V, the stability of the output current is high because the stack is operated in the region of ohmic polarization in which the flooding phenomenon is not obvious. However, the output current decreases with time under constant voltages of 0.45 V and 0.5 V because the stack is operated in the region of concentration polarization in which the air supply and the water removal become insufficient. When the PZT device vibrates in the cathode to alleviate the problems, the current balance is eventually restored.

The PZT-Stack generates maximum power when the constant load voltage is 0.5 V. At load voltages higher than 0.5 V, the stability of the output current is high because the device operates in the region of ohmic polarization. However, at load voltages lower than 0.5 V, the output current decreases with time such that it is difficult to obtain a current with long-term stability.

4.6. Influence of a degraded MEA on the PZT-Stack

In this section, the performance of the PZT-Stack is analyzed under a degraded working mode. In this test, a degraded MEA is applied to Bi-cell #2 of the PZT-Stack while the remaining bi-cells continue work normally.

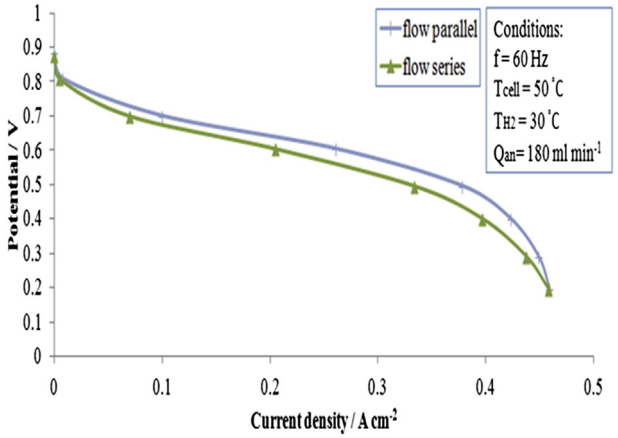

Fig. 13. The performance of the PZT-Stack at different intake modules in electrical parallel configuration.

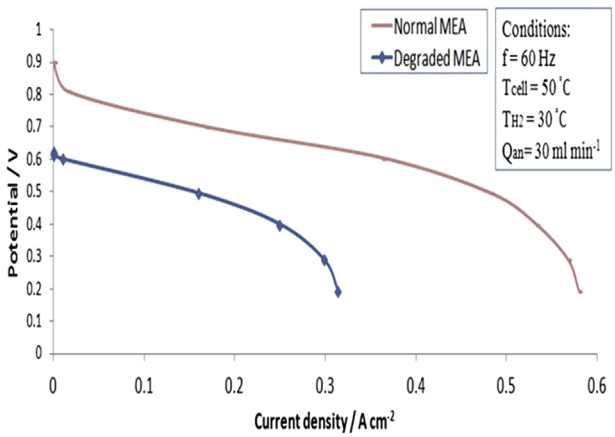

Fig. 15. The performance of the PZT-Stack applied with normal MEA and degraded MEA.

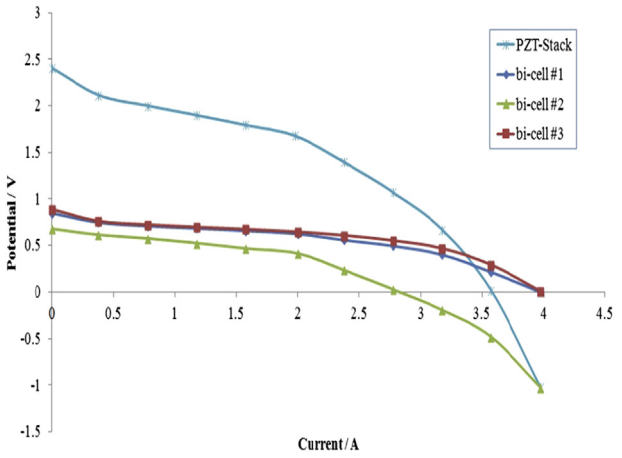

Fig. 16. The I–V curves of the PZT-Stack with a degraded MEA and the component bi-cells in electrical cascade configuration, $T_{H_2} = 30\ ^\circ C$, $T_{cell} = 50\ ^\circ C$, and $f = 60$ Hz.

The open-circuit voltage of the degraded MEA is only 0.6241 V, and the maximum current output of the degraded MEA is 2.5014 A, which is half that of a normal MEA, as shown in Fig. 15. Fig. 16 shows the I–V curves of the component bi-cells and the degraded PZT-Stack in the electrical cascade configuration, with parallel flow, $T_{H_2} = 30\ ^\circ C$, $T_{cell} = 50\ ^\circ C$, and $f = 60$ Hz. It is obvious that the I–V curve of Bi-cell #2 drops rapidly as the load current exceeds 2.4 A. Because the bi-cell is electrically parallel, the negative voltage output resulting from Bi-cell #2 with a degraded MEA means that an internal current exists inside the bi-cell, which may result from the voltage difference between the component cells. Although the PZT-Stack is arranged in an electrical cascade configuration, the stack system does not shut down if one of the component bi-cell fails due to the pseudo-bipolar design.

Fig. 17 shows the V–t curves of the PZT-Stack with a degraded MEA at different constant load currents in the electrical cascade configuration with $T_{H_2} = 30\ ^\circ C$, $T_{cell} = 50\ ^\circ C$, and $f = 60$ Hz. The stability of the output voltage is analyzed for period of 25 min, and observation shows that the presence of degraded MEA does not severely affect the performance of the stack under various load currents. At a constant load current of 2.4 A, the voltage variability is approximately 0.12 V. Although this result shows that the performance of the PZT-Stack decreases under a degraded working mode, the stack is still able to operate consistently in the electrical cascade configuration even if one of the component cells in the pseudo-bipolar design fails.

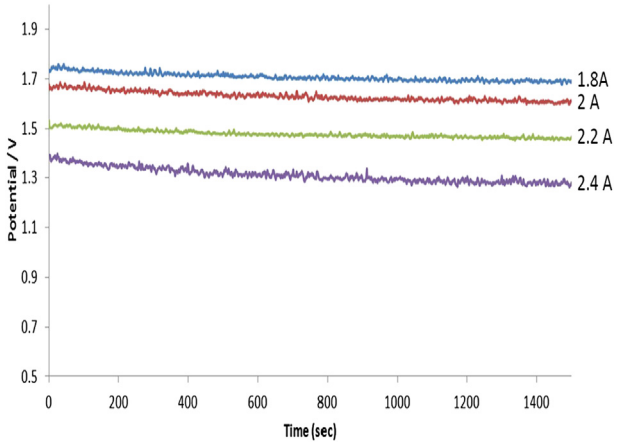

Fig. 17. The voltage stability of the PZT-Stack under various constant load currents with a degraded MEA in electrical cascade configuration, $T_{H_2} = 30\ ^\circ C$, $T_{cell} = 50\ ^\circ C$, and $f = 60$ Hz.

4.7. Net power of the PZT-Stack

The pseudo-bipolar design of the PZT-Stack requires only one PZT device for each L-PZT-D-type bi-cell to supply sufficient airflow for each component cell. The PZT device is a power-consuming device, and the required power is 0.6354 W, as measured by an AC power meter. In this study, the optimal performance of the PZT-Stack occurs at 4.4981 W with a PZT vibration frequency of 60 Hz, a cell temperature of 50 °C, a hydrogen humidification temperature of 30 °C and a hydrogen flow rate to each cell of 30 ml min^{-1} in the electrical parallel configuration. With respect to the power consumption of the PZT device, the maximum net power output of the PZT-Stack with three bi-cells is 3.8627 W.

5. Conclusion

An innovative pseudo-bipolar design for a PZT-Stack with three bi-cells has been successfully developed. The performance of the device was investigated under different operating conditions as well as under a degraded working mode. The major findings are as follows: (1) The PZT vibration frequency, cell temperature, and hydrogen humidification temperature are the major operating parameters for optimizing the performance of the L-PZT-D-type bi-cell in the PZT-Stack. The optimal bi-cell performance is obtained at a PZT vibration frequency of 60 Hz, $T_{cell} = 50\ ^\circ C$, and $T_{H_2} = 30\ ^\circ C$. (2) Under different PZT-Stack circuit modules, the maximum power density is 0.1874 W cm^{-2} in the electrical parallel and 0.1765 W cm^{-2} in the electrical cascade configuration. (3) Under the conditions of different intake modules on the anode, the maximum power density of the PZT-Stack is 0.1874 W cm^{-2} in parallel flow and 0.1652 W cm^{-2} in series flow. (4) The power consumption of the PZT device should be taken into consideration when determining the net power of the PZT-Stack. In this study, the maximum net power of the PZT-Stack in parallel flow was 3.8627 W in the electrical parallel configuration and 3.5699 W in the electrical cascade configuration. (5) The output current displays high stability at load voltages greater than 0.5 V because the stack is operated in the region of ohmic polarization. Therefore, the PZT-Stack should be operated at a load voltage of 0.5 V to obtain the maximum power and a current with long-term stability. (6) The electrical cascade configuration allows for an increase in the total output voltage but suffer from a severe weakness when one or more FCs fail. Because of the pseudo-bipolar design used in this study, the PZT-Stack does not exhibit open circuit behavior even if one of the component cells fails in the electrical cascade configuration. This finding will be a key to promoting the use of the PZT-Stack.

Acknowledgments

This research was funded by the National Science Council of the Republic of China (NSC 99-2221-E-002-126-MY2 and NSC 101-ET-E-002-009-ET)

Nomenclature

A_{PZ}	piezoelectric area (m^2)
AR	aspect ratio
Cn	nozzle conductivity coefficient
Cd	diffuser conductivity coefficient
D	channel opening width
f	frequency of PZT (Hz)
L	channel path

P	pressure (N m^{-2})
P_c	channel pressure
P_{in}	inlet pressure
P_{out}	outlet pressure
R	gas constant (J mol^{-1} K^{-1})
t	time (s)
T	temperature (K)
T_{H_2}	anode humidifier temperature (°C)
T_{cell}	cell temperature (°C)
V_{PZT}	motion equation of the piezoelectric device (m s^{-1})
Q	airflow rate
Λ	amplitude
θ	diffuser angle
ρ	density (kg m^{-3})
$\forall$	volume displacement (m^3)

References

[1] X. Yang, Z. Zhou, H. Cho, X. Luo, Sens. Actuators A 130-131 (2006) 531–536.
[2] A. Olsson, G. Stemme, E. Stemme, Sens. Actuators A 47 (1995) 549–556.
[3] A. Ullmann, Sens. Actuators A 69 (1998) 97–105.
[4] K.S. Yang, I.Y. Chen, C.C. Wang, Chem. Eng. Technol. 29 (2006) 703–710.
[5] Q. Yan, H. Toghiani, J. Wu, J. Power Sources 158 (2006) 316–325.
[6] J.H. Jang, H.C. Chiu, W.M. Yan, W.L. Sun, J. Power Sources 180 (2008) 476–483.
[7] J.S. Yi, T.V. Nguyen, J. Electrochem. Soc. 145 (1998) 1149–1159.
[8] S. Ge, C.Y. Wang, J. Electrochem. Soc. 154 (2007) B998–B1005.
[9] R. Jiang, D. Chu, J. Power Sources 93 (2001) 25–31.
[10] Fuel Cell Handbook, seventh ed., EG&G Technical Services, Inc., 2004.
[11] D. Candusso, A.D. Bernardinis, M.C. Péra, F. Harel, X. François, D. Hissel, G. Coquery, J.M. Kauffmann, Energy Convers. Manage. 49 (2008) 880–895.
[12] A.D. Bernardinis, M.C. Péra, J. Garnier, D. Hissel, G. Coquery, J.M. Kauffmann, Energy Convers. Manage. 49 (2008) 2367–2383.
[13] H.K. Ma, S.H. Huang, Y.Z. Kuo, J. Power Sources 185 (2008) 1154–1161.
[14] H.K. Ma, S.H. Huang, B.R. Chen, L.W. Cheng, J. Power Sources 180 (2008) 402–409.
[15] H.K. Ma, S.H. Huang, J. Fuel Cell. Sci. Technol. 6 (2009) 034501-1–034501-6.
[16] H.K. Ma, S.H. Huang, J.S. Wang, C.G. Hou, C.C. Yu, B.R. Chen, J. Power Sources 195 (2010) 1393–1400.
[17] H.K. Ma, J.S. Wang, Y.T. Chang, J. Power Sources 196 (2011) 3766–3772.
[18] H.K. Ma, J.S. Wang, W.H. Su, W.Y. Cheng, J. Power Sources 196 (2011) 7564–7571.
[19] K. Dhathathreyan, P. Sridhar, G. Sasikumar, K. Ghosh, G. Velayutham, N. Rajalakshmi, J. Hydrogen Energy 24 (1999) 1107–1115.